Optimization and Characterization of Home Made Ball Mill for Preparing Nano-sized Tungsten Heavy Alloy

H. Elshimy[1], Z.K.Heiba[1], S. F. Moustafa[2], Karimat El-Sayed[1]

[1]Physics Department, Ain Shams University, Cairo, Egypt
[2]Central Metallurgical R&D Institute, Cairo.

A mechanical home made ball mill was constructed in order to prepare nano crystallite size from 90W-7 Ni-3Fe heavy alloy. The parameters of the mechanical alloying process such as milling speed, milling medium, charge ratio and the filling ratio were varied in order to find their influence on the mill efficiency. It was found that the optimum parameters for the milling process at which the crystallite size decreased faster, the contaminations are minimized, the milling speed is adequate and the filling factor is justified are only obtained by using; rods as a milling medium instead of using balls, milling speed to be 175 rpm, charge ratio is 20:1 and the filling factor is 30 %. XRD was taken for all the samples milled at different times in order to see the different XRD pattern steps of the alloy formation. From Rietveld refinements it was possible to get the structural parameters, the crystallite size and the microstrain. These results were correlated with each other and with similar results obtained from the TEM. The energy dispersive X-Ray (EDX) results confirmed the weight percentage of the different elements and the homogeneity of the elemental powders in the resulting alloy.

2. Introduction

Nano-sized Tungsten heavy alloys are unique materials due to the combination of their high density, high strength, high ductility, high conductivity, high absorption capacity against X-ray and Gama-Ray and good machinability [1-3]. These properties have made these alloys a candidate for defense and civilian applications. They are widely used in many fields such as the medical, including radiation shielding, source holder, collimator, isotope container, nuclear syringe; the scientific, including tungsten heat sinks, oil drill, mine exploitation; the military, including bullet with sharpened head, balanced ball for missile and plane, etc; also in the sports, including golf, fishing, darts, yacht, racing car military [4-5]. Nano-crystalline tungsten alloy powders can be obtained by

mechanical alloying (MA) process, which is related to a high energy ball milling technique, which is the most widely used way to produce pre-alloyed powders because it is simple and effective [6-7].

The process of MA is closely related to ball milling conditions, such as the type and speed of ball milling, the ball-to-powder weight ratio (BPR) and the extent of filling the vial. Much research on modeling of the MA process has been conducted by many scientists in recent years and a theoretical relationship between the physical parameters of powder (such as deformation and temperature increase) and the technical parameters of ball milling have been established [8]. However, the comparisons of the model predictions with the experimental data are difficult. The experimental results are expressed as changes in composition, particle size, morphology, structure, or crystallinity, while models typically operate with such global parameters as number and energy of collisions between grinding media or local parameters such as coalescence and fracture probability and size distribution. Therefore, many experimental trials should be done to optimize the conditions of the mechanical alloying [9–10].

The aim of the present work is to build a mechanical alloying ball mill with optimum parameters in order to obtain nano crystallite size for the tungsten heavy alloy.

3. Experiment

3.1. Optimization of the Milling Conditions

The mill consists of two rotators connected to a motor of maximum rotation speed 1000 rpm and the vial rotates at the same speed as the tray, but in the opposite direction. The vial is a cylinder of stainless steel with diameter 3.8 cm and height 7.5 cm. A rubber ring placed on the cover ensures the tightness of the vial, which is filled by a purified argon atmosphere. A cooling system consists of several fans used to reduce the temperature rising during milling. The mill and the vial are represented in Fig.(1).

As it was previously mentioned, the process of MA is closely related to ball milling conditions, such as the type and speed of ball milling, the ball-to-powder weight ratio and the extent of filling the vial. The goal was to obtain a nano-homogeneous powder without contamination and avoid the agglomeration on the milling medium, and also prevent the oxidation of the powders, all of that to be obtained in less time possible. The optimization was done mainly on the following parameters: milling medium, milling atmosphere, rods diameters, milling speed, charge ratio, filling factor.

Fig. (1): The Home made ball mill

The mechanical alloying was processed first in air then in argon atmosphere. The milling mediums were hardened balls once and Stainless steel rods once. The balls diameter was 10 mm and the rods diameters were varied from 2 to 6 mm. The milling speed was varied from 150 rpm to 250 rpm, charge ratio was varied from 10 to 30 in weight and filling factor was varied from 20 to 50 in volume fraction. In this manner, we have chosen the best conditions for the preparation of the tungsten heavy alloys nanoparticles.

The Tungsten powder of 2.46 μm, nickel powders of 2.3 μm and iron powder of 2.1 μm in average size with weight percentage 90W-7Ni-3Fe were mechanically alloyed in the mill to optimize the mill for the preparation of tungsten heavy alloy.

3.2. Characterization and Analysis

After various times of milling, small amounts of mechanically alloyed powders were taken from the container and characterized by X-ray diffraction (XRD) using the PHILIPS® MPD X'PERT diffractometer which has the Bragg-Brentano geometry. The X-ray tube used was a Copper-tube operating at 40 KV and 30 mA, the divergence slit angle was 1^{o}, the receiving slit was 0.1^{o}, step scan size 0.03 and the scan step time was 5 seconds.

The microstructure was examined by scanning electron microscopy assisted with energy dispersive X-ray spectroscopy (SEM-EDX) at an operation voltage of 30 KV. Transmission electron microscopy (TEM), type JEOL TEM 1230 with an operating voltage of 120 KV was used in this work.

In the present study, we have adopted the Rietveld's powder structure refinement analysis [11], of X-ray powder diffraction data to obtain the structural and the microstructural parameters, such as the lattice parameters, particle size, rms lattice strain and the phase concentration (volume/weight fraction). The structural and microstructural characterization of unmilled and all the ball-milled powder samples have been made by employing the Rietveld software MAUD 2.074.

Since the resulting broadening is due to two factors, Physical broadening (crystallite size and lattice strain) and instrument broadening. So, in order to know the crystallite size correctly, the instrumental broadening was determined using the standard reference material LaB6. The care was taken during collection of XRD patterns so that the experimental conditions are the same for the standard material and the samples studied.

The background of each pattern was fitted by a polynomial function of degree four. The experimental profiles were fitted with the most suitable pseudo-Voigt analytical function [12], because it takes individual care for both the particle size and strain broadening of the experimental profiles.

The least-squares procedures were adopted for minimizing the difference between the observed and calculated powder diffraction patterns and the minimization was carried out by using the reliability index parameter, R_{wp} (weighted residual error), and R_B (Bragg reliability factor). The goodness of fit (GoF) is established by comparing R_{wp} with the expected error, R_{exp}. The refinement was continued until convergence was reached and the value of the quality factor (GoF) approached acceptable values.

4. Result and Discussion

4.1. Optimization of the Milling Conditions

4.1.1. The Milling Medium

90W-7Ni-3Fe powders were mechanically alloyed for 20, 40 and 60 hrs using hardened balls of diameter 10 mm and stainless steel rods of 4 mm respectively. The milling speed was 211 rpm, the charge ratio was 20:1 and the filling factor was 40%.

Figure (2-a) shows the crystallite size of the mechanically alloyed powders using hardened balls and stainless steel rods. The decrease in the crystallite size by using the stainless steel rods was faster than that by using the hardened balls, more over the contamination percentage of Fe contents was also smaller in case

of stainless steel rods Fig. (2-b). Accordingly, the stainless steel rods were recommended to be used in this work.

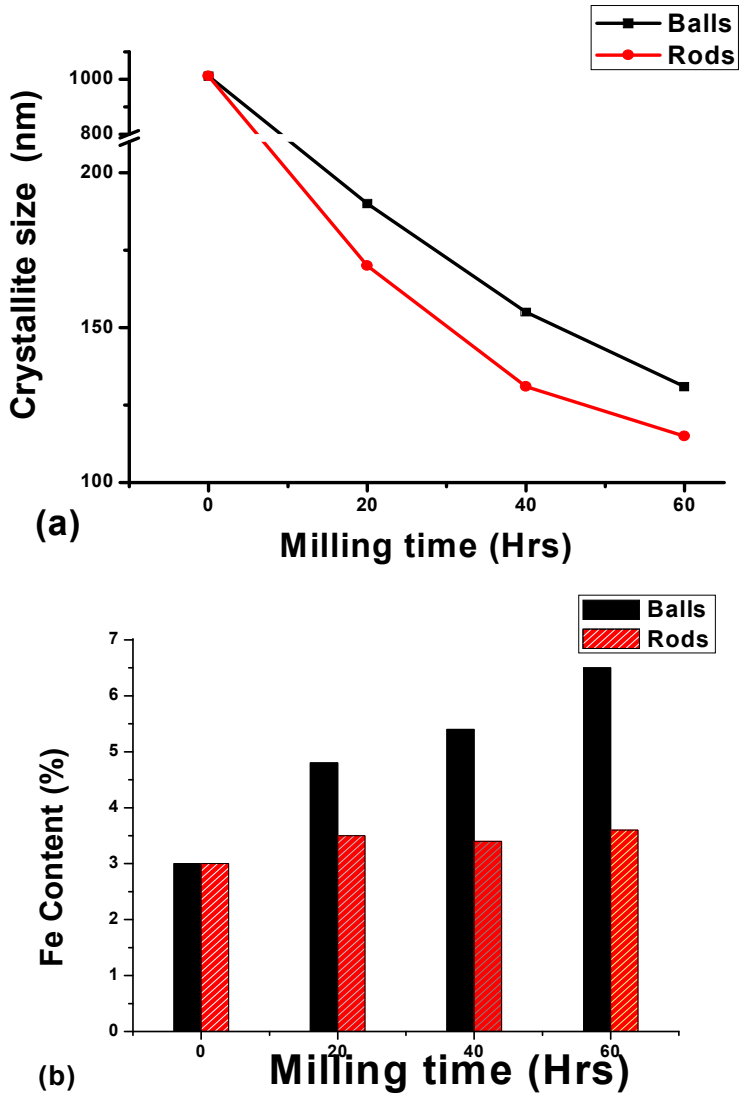

Fig. (2): The effect off the milling medium on the milling process (a) the change of the crystallite size, (b) the Fe contamination

Three different rods sizes of 2, 4 and 6 mm in diameter were used in order to select the optimized one. Fig. (3) shows the crystallite size of mechanically alloyed powders with rods diameters 2, 4 and 6 mm for 20 and 60 hrs. It's clear that the 6 mm rods are desirable since the larger weight of the balls will transfer more impact energy to the powder particles.

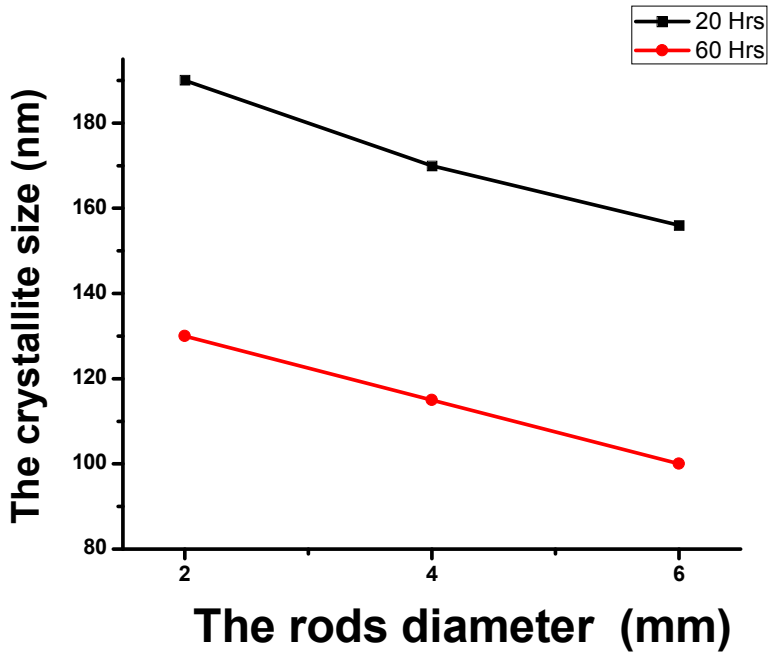

Fig. (3): The effect of the milling rod diameters on the milling process

4.1.2. The milling speed

The theoretical maximum milling speed for mechanical alloying by using cylindrical ball mill can be obtained when the gravity and centrifugal force are balanced as indicated in eq.(1).

$$m\,g = m\,r\,\omega^2 \qquad (1)$$

where m is mass of a milling ball, g is gravitational constant, r is radius of milling vial and ω is angular velocity of ball mill. According to Eq.(1), the theoretical maximum milling speed was calculated as 211 rpm for the stainless steel rods. Fig. (4) shows the crystallite size of mechanically alloyed powders for 20 and 60 hrs with milling speed 150, 175, 211 and 250 rpm.

When the milling speed was 175 rpm which is close to the calculated theoretical speed, the collision between the rods and the powders occurred actively and the elemental powders were mechanically alloyed effectively. The difference between the theoretical and experimental maximum speed is due to the filling medium, where the medium in the first was air and the medium at our experiment was Argon.

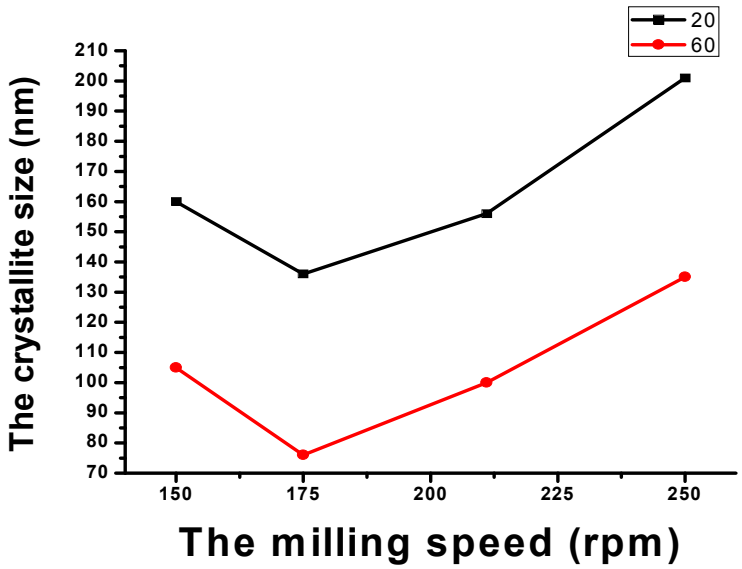

Fig. (4): The effect of the milling speed on the milling process

4.1.3. The Charge Ratio

Normally, the intensity of the shocks is directly proportional to the charge ratio; higher is this ratio, higher is the frequency of the shocks and, thus, the milling is more energetic. In this work, we have varied the rods to powder ratio from 10 : 1 to 30:1 at milling speed of 175 rpm for 20 and 60 hrs.

Figure (5-a and 5-b), show the effect of the charge ratio on the milling process, which shows that, at high rods to powder ratio (RBR) the reduction in the size takes place faster because of an increase in the weight proportion of the rods but also the contamination from the rods increased. But at 20: 1 rods to powder ratio the level of the contamination is less than that of the 30:1 ratio and the rate of size reduction is nearly the same. So 20:1 is recommended ratio for our mill.

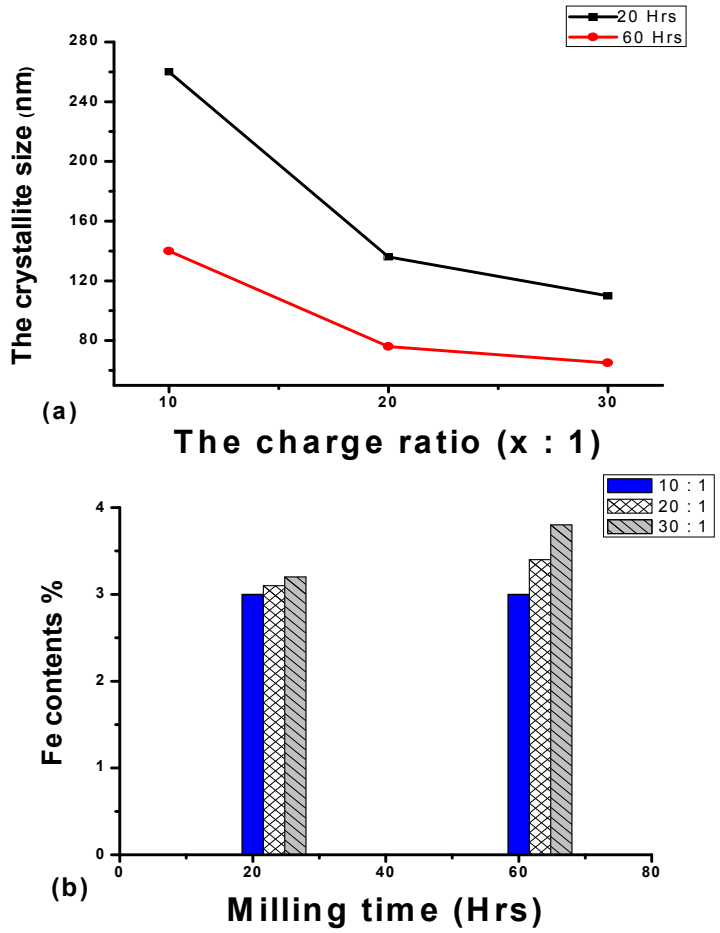

Fig. (5): The effect of the charge ratio on the milling process (a) on the crystallite size, (b) on the Fe contamination

4.1.4. The Filling Factor

Since alloying among the powder particles occurs mainly due to impact forces exerted on them by steel rods, so it is necessary to optimize the space volume in order to allow the rods to hit the powder particles with its maximum force. Therefore, the extent of filling the vial with the powder and the rods is optimized by varying it from 20% to 50% at the previous optimized parameters for 60 hrs.

Figure (6), shows the effect of the filling factor on the milling process, which shows that, the crystallite size was decreased as the filling factor increased up to 30% where above it, the efficiency of the mill decreased. Also, the level of

the contamination was increased as increasing the filling factor above the 30% capacity. So 30% filling factor is desirable.

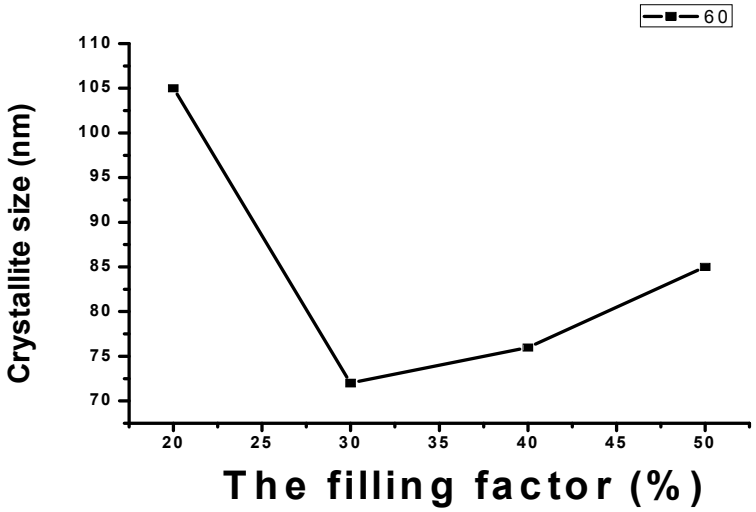

Fig. (6): The effect of the filling factor on the milling process.

4.2. Structural and microstructural analysis

Using the optimized conditions, the 90W-7Ni-3Fe powder samples were mechanically alloyed for 50, 100, 150, 200 and 400 hrs using stainless steel rods of diameter 6 mm, milling speed of 175 rpm, powder charge ratio of 20:1 and filling factor of 30%. To reduce oxidation of powders during mechanical alloying, the mechanical alloying was performed under high purity of argon atmosphere.

Figure (7), shows the X-ray diffraction patterns of the mechanically alloyed powder of 90W-7Ni-3Fe for different milling time. It can be seen that, the diffraction peaks become gradually broadened and the peak intensities decreased with the increase of milling time. The peak broadening detected in the patterns suggests that both the crystallite size of the mixed powders and the microstrain are significantly affected by the mechanical milling. Also no new other phases or foreign diffraction peaks were observed at different milling time as seen in Fig.(7).

All the unmilled and ball-milled XRD patterns are analyzed by using MAUD program [13]. Some of the selected refined patterns are presented in Fig. (8). The Bragg residual factor, R_B and The goodness of fitting, GoF, values of all the fitted patterns lie within 4.6-7.5 % and 1.4-2.9 respectively as listed in Table (1).

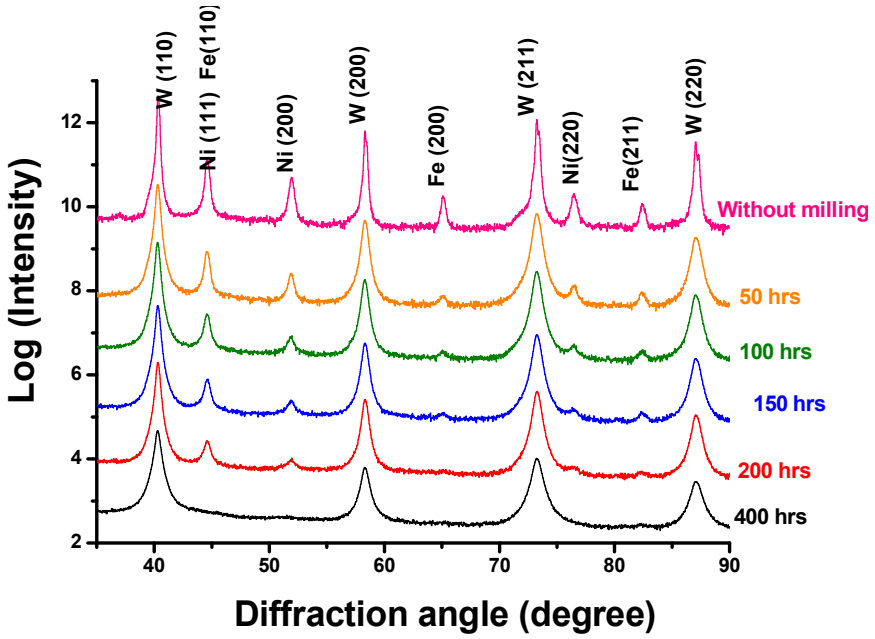

Fig. (7): XRD patterns for 90W-7Ni-3Fe (wt%) powders milled for different times

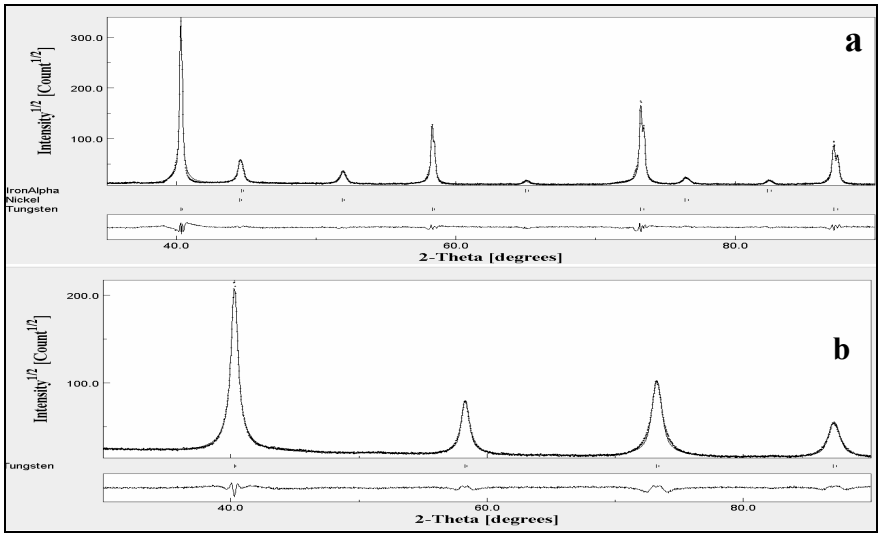

Fig. (8): Observed (.) and calculated (–) X-ray powder diffraction patterns of unmilled (a) and 400 Hrs milled powders (b) revealed by Rietveld powder structure refinement.

Table (1): The Bragg reliability factor and the goodness of the fitting values of all the refined patterns

Milling time (hrs)	The Bragg factor (R_B) %	The goodness of fitting (GOF)
0	7.1700	2.5
50	7.5000	2.9
100	6.9000	2.7
150	7.0000	2.7
200	6.6000	2.5
400	4.6000	1.4

Figure (9-a), shows the influence of milling time on the tungsten crystallite size. After 50 hrs, the mechanical milling leads to a fast decrease of the crystallite size to 81 nm. As the milling time increased the trend of the rate of the crystallite decrease becomes less. At 200 hrs the crystallite size is nearly the same as that of 150 hrs, which suggests that the rate of milling is approximately equal to the rate of agglomeration. Further decrease in crystallite size occurs slowly up to about 25 nm after 400 hrs.

Fig. (9-b), shows the influence of milling time on the microstrains of the tungsten powders. As can be seen, the lattice strain exhibits an increase to about 0.23% at 100 hrs and this is due to the formation of lattice defects during milling. Further milling causes the lattice strain to decrease, which suggest that at longer time of milling heat energy is generated by the mechanical impact of the steel rods and during collision between particles fast grain boundary diffusion process occurs as demonstrated by Fig. 10-b and 10-c , more over the heat generated will act as annealing effect i.e minimizing the strains [14].

Fig. (10a, b and c), show the microstructure of the milled powders at different time by TEM. Fig. (10-a), shows the sample milled at 50 hrs which has a nearly spherical morphology with average size 97 nm and this value is also in agreement with that of the XRD analysis for the same sample. For further milling a significant amount of agglomeration is observed as shown in Fig. (10-b), after milling time of 150 hrs and in Fig. (10-c), after milling time of 200 hrs. This is known as nanopowders agglomeration [15], which is agglomeration of fine nanocrystallite.

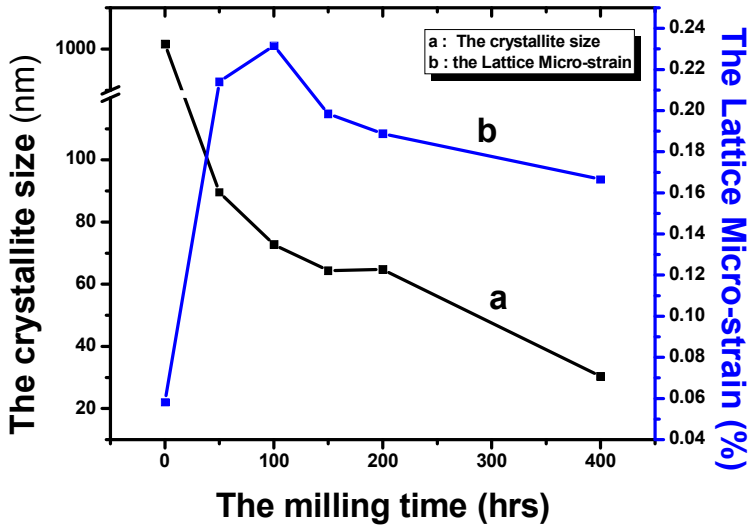

Fig. (9): The effect of the milling time on the crystallite size (a) and on the microstrain (b)

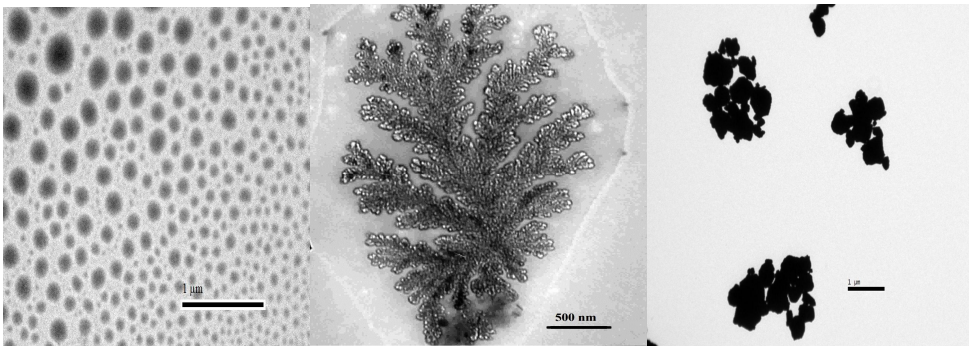

a **b** **c**

Fig. (10): TEM for powders milled for 50 hrs (a), 150 hrs (b) and 200 hrs (c)

Fig. (11), shows the volume fraction of different phases with increasing milling time calculated from XRD. By increasing the milling time the tungsten content increases and Ni and Fe content decreases. Several trials were made suggesting the diffusion of the Ni and Fe atoms into the W lattice either by substitution or interstitial but the results obtained from Rietveld refinement did not show any change in the tungsten lattice parameter as seen in Fig. (12). This suggests that the Ni and Fe atoms may form amorphous phase on the boundary of the tungsten particles. This was confirmed by Reitveld refinement for W, Fig. (8-b).

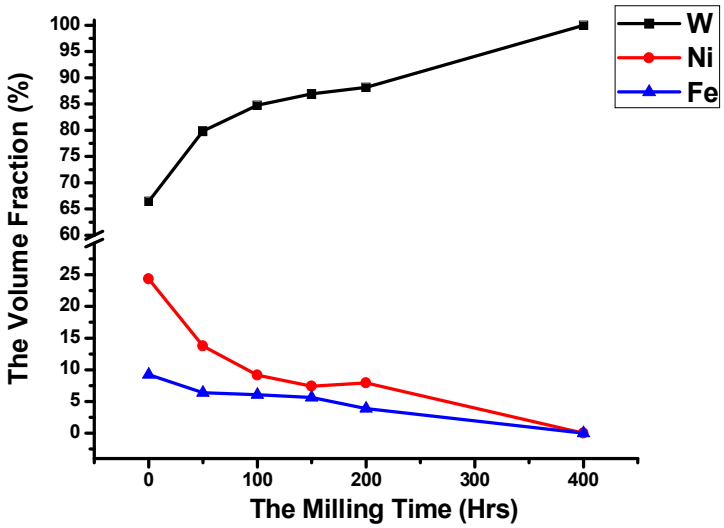

Fig. 11 The variation of the volume fraction with milling time

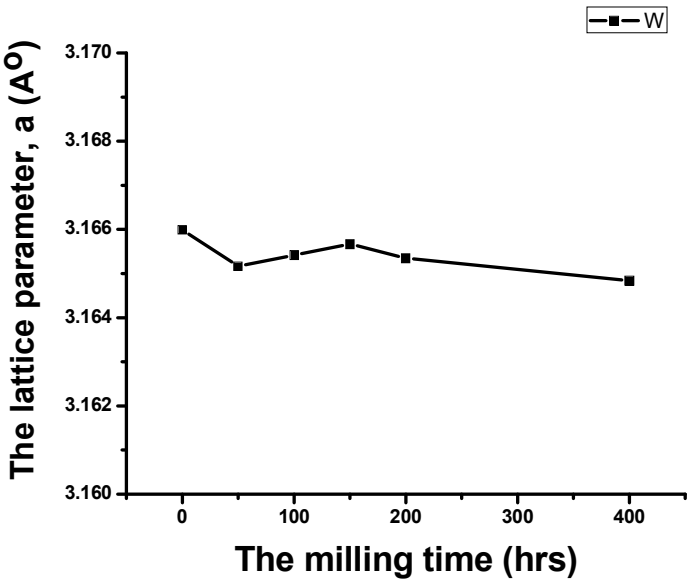

Fig. (12): The variation of the lattice parameter with milling time.

Fig. (13) shows EDX spectrum of the elemental composition of the synthesized W–Ni–Fe ternary alloy after milling for 400 hrs. The elemental analysis was taken randomly from different locations on the sample. The results of the percentage of the element are shown in Table (2).

Table (2): Element contents at different regions of 90W-7Ni-3Fe alloy after milling 400 hrs

Elements / Regions	W %	Ni %	Fe %
Full Scan	90.55	6.35	3.10
Region A	89.30	6.70	4.00
Region B	90.26	6.27	3.47
Region C	90.65	6.05	3.30

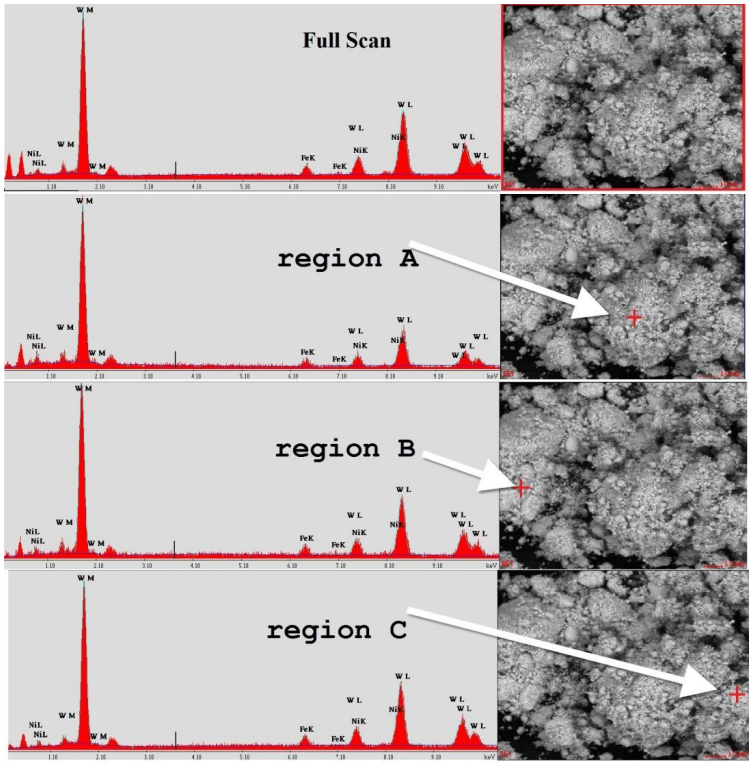

Fig (13): The SEM and EDX for the 90W-7Ni-3Fe alloy after milling 400 hrs

5. Conclusion

In this work we were able to construct a home made ball mill of reasonable size and optimized conditions at which it works at its maximum efficiency. Variable crystallite sizes in nano range up to 25 nm were obtained. At the beginning of milling, the mechanical milling leads to fast decrease in the crystallite size and an appreciable increase in the lattice strain. Further milling

causes the lattice strain to decrease due to the annealing effect and causes the rate of the crystallite decrease to be less. The changes in morphology of the crystallite size were demonstrated at different milling time by using the TEM. After milling time of 150 hrs, a significant amount of agglomeration started to appear. The chemical composition of the synthesized 90W-7Ni-3Fe alloy was analyzed by EDX and the result revealed that all the elements were uniformly distributed through the alloy and they were all of the same percentage in composition as those of the starting alloy.

References

1. M.A. Yun-zhu, HUANG Bai-yun, *LIU Wen-sheng. The Powder Metallurgy Industry*, **15**(5): 46 (2005).

2. FAN Jing-lian, HUANG Bai-yun, *QU Xuan-hui. Trans Nonferrous Met. Soc. China*, **10** (1): 57 (2000).

3. H. J. RGU, S H. HONG, W. H. BACK., *J. Mater. Proc. Tech*., **(67)**: 292 (1997).

4. W.D. Cai, Y. Li, R.J. Dowding, F.A. Mohamed, E.J. Lavernia, *Rev. Particulate Matter*., **3**, 71 (1995).

5. Z.-W. Zhang, J.-E. Zhou, S.-Q. Xi, G. Ran, P.-L. Li., *Mater. Sci. Eng. A* **379**, 148 (2004).

6. M.L. Ovecoglu, B. Ozkal, C. Suryanarayana, *J. Mater. Res*. **11**, 1673 (1996).

7. MA Yun-zhu, HUANG Bai-yun, FAN Jing-lian, XIONG Xiang, *WANG Deng-long. The Powder Metallurgy Industry*, **14**(5): 17 (2004).

8. A. Concas, N. Lai, M. Pisu, G. Cao., *Chemical Engineering Science*, **(61):** 3746 (2006).

9. T. S. Ward, W. Chen, M. Schoenitz, R. N. Dave, E. L. Dreizin, *Acta Materialia*, **(53):** 2909 (2005).

10. D. Maurice, T. H. Courtney, *Metal and Mater Transactions*, **(26A)**: 2431 (1995).

11. L. Lutterotti, P. Scardi, P. Maistrelli, *J. Appl. Crystallogr*. **25**, 459 (1992).

12. R.A. Young, D.B. Wiles, *J. Appl. Crystallogr*., **15**, 430 (1982).

13. L. Lutterotti, *MAUD version*, **1**. 85 (2002)

14. H. Dutta, S.K. Pradhan, M. De, *Materials Chemistry and Physics*, **74**, 167 (2002).

15. B.D. Fahlman, *Material chemistry Springer*, (2007).